

PAPER • OPEN ACCESS

Heterodyne interferometry at ultra-high frequencies with frequency-offset-locked semiconductor lasers

To cite this article: Robert Kowarsch and Christian Rembe 2020 *Meas. Sci. Technol.* **31** 075201

View the [article online](#) for updates and enhancements.

You may also like

- [A primary standard for the volume flow rate of natural gas under high pressure based on laser Doppler velocimetry](#)
B Mickan and V Strunck
- [Decarbonizing US passenger vehicle transport under electrification and automation uncertainty has a travel budget](#)
Abdullah F Alarfaj, W Michael Griffin and Constantine Samaras
- [Accurate and precise calibration of AFM cantilever spring constants using laser Doppler vibrometry](#)
Richard S Gates and Jon R Pratt

Heterodyne interferometry at ultra-high frequencies with frequency-offset-locked semiconductor lasers

Robert Kowarsch  and Christian Rembe

Institute of Electrical Information Technology, Department of Applied Metrology, Clausthal University of Technology, Leibnizstraße 28, 38678 Clausthal-Zellerfeld, Germany

E-mail: kowarsch@iei.tu-clausthal.de

Received 15 January 2020, revised 17 February 2020

Accepted for publication 24 February 2020

Published 9 April 2020



CrossMark

Abstract

Modern broadband telecommunications require microelectromechanical filters which mechanically vibrate at ultra-high frequencies up to several gigahertz. Heterodyne interferometers, so-called laser-Doppler vibrometers (LDVs), provide a sensitive and contactless measurement technique for vibrations in such filters, but are limited in GHz heterodyning by the efficiency drop of acousto-optic frequency shifters. Heterodyning by frequency-offset locking of two lasers in an optoelectronic phase-locked loop (OPLL) overcomes this limitation. This is demonstrated with our LDV setup with heterodyning up to 1.4 GHz via offset locking of two semiconductor lasers at visible wavelength. The experiments show a vibration-amplitude resolution of less than 1 pm per $\sqrt{\text{Hz}}$ for frequencies higher than 50 MHz up to 700 MHz. The bandwidth is only limited by our photodetectors. This amplitude resolution already qualifies our LDV for vibration measurement of microelectromechanical filters at ultra-high frequencies. We present a comprehensive model for the vibration-amplitude resolution of a LDV with this technique including the laser linewidths, the OPLL transfer function, and interferometer delays. The experiments with our LDV validate the model predictions from numerical simulations. Finally, we discuss the collapse of the heterodyne carrier at vanishing mutual coherence due to interferometer delays, the transition to shot-noise-limited detection, and provide design recommendations.

Keywords: heterodyne interferometry, optical phase-locked loop, MEMS testing, vibration measurement

(Some figures may appear in colour only in the online journal)

1. Introduction

With the steadily-increasing demands for broadband telecommunications, highly selective radio-frequency microelectromechanical (RF-MEM) filters have been developed with microacoustic vibrations at frequencies up to several GHz [1] and vibration amplitudes of few nanometers or less. The

sensitive and contactless measurement of RF vibrations and the operating deflection shape of these microelectromechanical systems (MEMS) is vital for quality control and optimization.

Laser-interferometric techniques are well established in vibration analysis of RF-MEMS in the gigahertz range. The vibration measurement relies on the laser-Doppler effect, which transduces the motion at the measurement spot into a phase modulation of the scattered laser light. Therefore, this class of interferometers is often referred as laser-Doppler vibrometers (LDVs) [2, 3]. Homodyne LDVs directly measure the phase modulation in the baseband and are capable to measure vibrations up to more than 10GHz



Original Content from this work may be used under the terms of the [Creative Commons Attribution 4.0 licence](https://creativecommons.org/licenses/by/4.0/). Any further distribution of this work must maintain attribution to the author(s) and the title of the work, journal citation and DOI.

[4, 5]. However, homodyne LDVs are sensitive against photodetector nonlinearities and reflectivity modulations, which typically occur at edges of the structure or imperfections. The reconstruction of the vibration in amplitude and phase requires elaborate stabilization and calibration [6]. Therefore, a general uncertainty for the vibration amplitude cannot be derived [7].

In heterodyne LDVs, a carrier frequency in the measurement signal is conventionally introduced by shifting the frequency of one of the two interfering beams. Thus, the phase modulation due to Doppler shifts results in a Bessel spectrum around the heterodyne carrier in the photodetector signal. For an unambiguous reconstruction of small vibration amplitudes, the heterodyne-carrier frequency must exceed the maximum vibration frequency. Further, the electronic bandwidth has to be larger than twice the maximum vibration frequency. Obeying these requirements, heterodyne LDVs are insensitive against intensity modulations and provide a defined uncertainty for the vibration amplitude. However, this imposes ambitious demands on both the heterodyning technique and the bandwidth of photodetectors. Further, the small acoustic wavelengths at UHF frequencies require high-resolution or even super-resolution microscopy in combination with the LDV. In previous applications, we proposed absorbance-modulation nanoscopy in reflection [8] and studied its potential [9].

Conventionally, heterodyning in LDVs is introduced by frequency shifting in acousto-optic devices. However, conventional paratellurite frequency shifters are inefficient for shifting higher than 409 MHz [10]. To measure RF vibrations, published approaches employ multiple beam passes through the acousto-optics [11], which suffers from losses due to diffraction efficiency. Those approaches can be combined with deconvolution of the spectrum from the imaged lower sideband of the phase modulation [11], which requires a-priori knowledge, or evaluation of only the lower (imaged) sideband [12]. With this single-sideband evaluation, the heterodyne LDV cannot discriminate phase and intensity modulations anymore.

The technique of heterodyning by frequency-offset locking between two or more laser sources with an optoelectronic phase-locked loop (OPLL) has established itself in many fields of application, e.g. coherent optical telecommunication [13–15], swept-frequency sources for ranging [16], coherent combining [17], terahertz photonics [18], gravitational wave detection [19, 20], atomic clocks [21], frequency metrology [22, 23], and interferometry [24]. In previous conference publications [25, 26] we already presented the potential of offset locking of two semiconductor lasers as a flexible technique for heterodyning in laser-Doppler vibrometry in the gigahertz regime. Therefore, LDV can overcome the limitations of acousto-optic frequency shifting and achieve unambiguous measurement capability in the gigahertz regime.

In this work, we present a comprehensive model for the achievable vibration-amplitude resolution with offset-locked semiconductor lasers, which expresses the vibration-amplitude resolution limit based on the differential-phase noise determined by the OPLL. In our model, we consider frequency noise of the incorporated lasers, the OPLL transfer

function, and interferometer delays. Hitherto, published modeling approaches for the differential-phase noise from an OPLLs assume ideal OPLL transfer function [17] or simplified transfer function of the OPLL without intra-loop delays [27] with the aim to quantify the generated mutual coherence.

We validate the model predictions theoretically and with experimental data from our LDV with frequency-offset-locked semiconductor lasers. We further discuss the heterodyne carrier strength and its collapse, when the mutual coherence between the interfering beams vanishes due to long optical path differences in the interferometer setup. Finally, we express the transition frequency for shot-noise-limited detection in dependence on the linewidth of the lasers. The model and the discussion shows the general potential and limitations of heterodyning with offset-locked lasers for laser-Doppler vibrometry and it gives valuable estimates for the LDV design.

2. Laser-Doppler vibrometer with heterodyning via offset-locked lasers

2.1. Concept of heterodyning with offset-locked lasers

A typical LDV comprises the optical setup of a Mach–Zehnder interferometer with a broadband acquisition of the light phase difference [2], shown in figure 1(a). Generally in interferometers, a portion of a laser source (reference beam) is interfered with another portion of usually the same laser source (measurement beam), which contains phase modulations representing the measured quantity.

At the photodetectors (PD1-2), the measurement beam (power P_m and mean frequency ν_m) and the reference beam (power P_r and frequency ν_r) interfere and generate the photocurrent signal:

$$i(t) = 2\chi\mathcal{S}\sqrt{P_m P_r} \cos[2\pi(\nu_m - \nu_r)t + \Delta\varphi(t)] \\ = \hat{i} \cos[2\pi\nu_c t + \Delta\varphi(t)] \quad (1)$$

with the interference efficiency χ , the photodetector sensitivity \mathcal{S} , and the photocurrent amplitude \hat{i} . The differential-phase modulation $\Delta\varphi(t)$ contains both deterministic and stochastic phase modulations. A LDVs relies on deterministic phase modulation caused by the temporal modulation of the optical path difference due to the laser-Doppler effect. From this, the phase derivative $\dot{\varphi}_{\text{vib}}(t)$ is proportional to the sample velocity $\dot{s}(t)$ (in direction of the measurement beam) with [3]:

$$\frac{\dot{\varphi}_{\text{vib}}(t)}{2\pi} = \frac{2\dot{s}(t)}{\lambda} \quad (2)$$

with the wavelength λ and the velocity c of light. In heterodyne LDVs, the frequency difference $\nu_c = |\nu_m - \nu_r|$ is non-zero, which is denominated as heterodyne carrier frequency [3]. This frequency shift is conventionally introduced by an acoustooptic device (Bragg cell).

Only some degree of statistical similarity between the temporal phases of the interfering beams is required to generate an interference signal [28]. Thus, interference also occurs

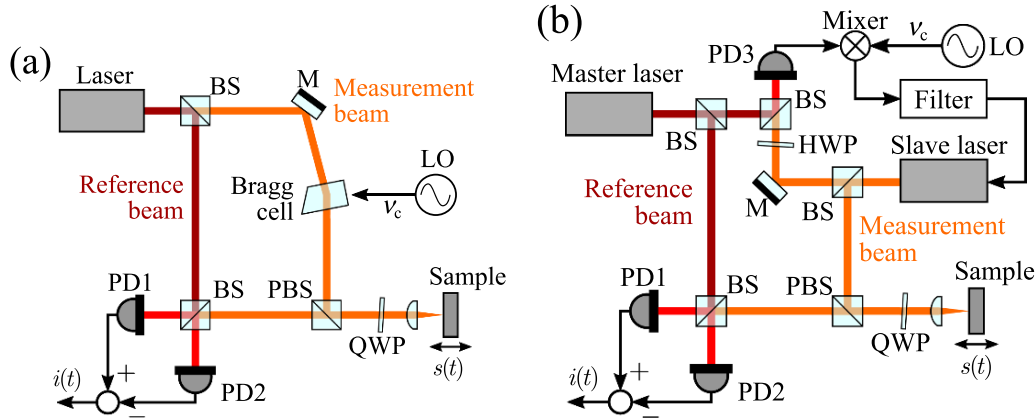


Figure 1. (a) Schematic setup of a heterodyne LDV of Mach-Zehnder type using a single laser in comparison with (b) the proposed LDV with offset-locked lasers by an optoelectronic phase-locked loop. LO is local oscillator, BS is non-polarizing beam splitter, PBS is polarizing beam splitter, QWP is quarter-wave plate under 45 deg, HWP is half-wave plate under 45 deg, M is mirror, and PD is photodetector.

between different laser sources [29]. However, a significant degree of mutual temporal coherence must exist to provide an exploitable heterodyne carrier for interferometry. Coupling the interfering lasers in an optoelectronic phase-locked loop (OPLL), shown in figure 1(b), can achieve this mutual coherence. Therefore, a photodetector (PD3) detects the phase (and frequency) difference (‘beat’) between the free-running master and the slave laser. The phase difference is compared by a mixer to the desired heterodyne carrier frequency ν_c generated by a signal generator (local oscillator). A negative feedback to the tunable slave laser controls the slave laser output to the offset frequency ν_c . In lock state, the phase lock reduces differential-phase noise within its bandwidth [30]. For interferometry, the master laser emits the reference beam and the slave laser the measurement beam. One could argue that the phase difference for the OPLL can also be measured at the interferometer photodetectors (PD1+2). However, this would have the disadvantages that (1) a lock would be only possible with good reflection at the sample, (2) any fluctuations of the surface reflectivity and the returning wavefront (spatial coherence) during measurement would impair the stability of the lock, and (3) the low-frequency bandwidth must be sacrificed for control and is not available for vibration measurements. The latter is of minor interest for our scope.

2.2. Controller modeling for optoelectronic phase-locked loop

For the expression of the residual differential-phase noise, the nonlinear differential equation of the OPLL can be linearized in the operating point ($\nu_M - \nu_S = \nu_{LO} = \nu_c$) for small phase fluctuations (see figure 2). This derivation can be found in standard textbooks [30]. The phase of the slave laser φ_S in the operating point is locked to the sum phase of the master laser and the local oscillator $\varphi_M + \varphi_{LO}$. The phase noise of the slave laser is modeled with an additive output disturbance φ_S^{fr} . Thus, the controller equation in Laplace domain is [30]

$$\varphi_S(s) \approx H(s) [\varphi_M(s) + \varphi_{LO}(s)] + [1 - H(s)] \varphi_S^{fr}(s) \quad (3)$$

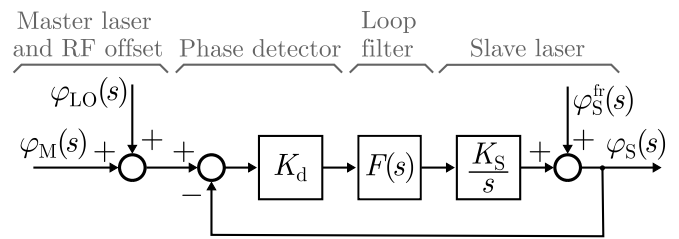


Figure 2. Circuit diagram of the linearized OPLL operation.

with the transfer function $H(s) = G_{OL}(s)/[1 + G_{OL}(s)]$ and the open-loop transfer function $G_{OL}(s)$. The open-loop transfer function includes all intra-loop components and delays: The complete gain K_d from phase detection (in the photodetector (PD3) and mixer), the loop filter with its transfer function $F(s)$, and the slave laser as controlled oscillator with the integrating transfer function K_S/s . The phase-noise contribution of the local oscillator is neglected for simplicity, since it is low compared to semiconductor lasers.

From (3) it can be directly concluded that high gains of the open loop suppress the phase fluctuations φ_S^{fr} of the free-running slave laser within the loop bandwidth. Instead, the locked phase of the slave laser φ_S follows the phase of the master laser φ_M and the local oscillator φ_{LO} . This transfer of the coherence properties of the master laser to the slave laser by the OPLL (within the loop bandwidth) is also denominated ‘coherence cloning’ [17].

2.3. Noise-equivalent vibration-amplitude resolution

Resolution and sensitivity of LDVs are sometimes used in misleading ways. The sensitivity of a LDV is strictly defined from the linear relation of the Doppler effect in (2). Whereas the resolution of a LDV defines the smallest variation of the measurand (vibration amplitude) the LDV can detect. The resolution for vibration amplitudes is usually expressed by the noise-equivalent vibration amplitude \hat{s}'_{ne} at 1 Hz resolution bandwidth (RBW) (in $m/\sqrt{\text{Hz}}$) [3]

$$\hat{s}'_{\text{ne}}(f_{\text{vib}}) = \frac{\lambda}{2\sqrt{2\pi}\sqrt{\text{SNR}'(f_{\text{vib}})}} \quad (4)$$

with the signal-to-noise ratio SNR' at 1 Hz RBW at the vibration frequency f_{vib} .

The typical noise sources in LDV measurement can be found in various textbooks [3]. It is beneficial to design an LDV that shot noise is dominant. These shot-noise-limited LDV measurement provides noise-equivalent vibration amplitudes down to femtometer/ $\sqrt{\text{Hz}}$ [3]. The SNR' at 1 Hz RBW, governed by power spectral densities (PSD) of shot noise $S_{i,\text{SN}}$ and differential-phase noise $S_{i,\text{PN}}$, is

$$\text{SNR}'(f_{\text{vib}}) \approx \frac{\hat{i}^2/2}{S_{i,\text{PN}}(\nu_c \pm f_{\text{vib}}) + S_{i,\text{SN}}}. \quad (5)$$

For simplicity, we assume that the significant intensity noise of semiconductor lasers is ideally suppressed by balanced photodetection.

3. Model for heterodyning via offset-locked lasers

3.1. Photocurrent noise from differential-phase noise

The following model approximates the resulting photocurrent-PSD (at PD1/2 in figure 1(b)) from differential-phase noise of two laser sources. The beams of the two lasers interfere on photodetector PD3 with an optical path difference OPD_{PD3} in respect to emission. Within the interferometer, the laser beams interfere with OPD_{PD12} on the photodetectors PD1 and PD2. Thus, the time difference between these interferences results in the interferometer delay $T_{\text{LDV}} = (\text{OPD}_{\text{PD12}} - \text{OPD}_{\text{PD3}})/c$. If the optical path differences are equal ($T_{\text{LDV}} = 0$), the interferometer signal without laser-Doppler shift resembles the controlled beat signal. As the beam paths can differ in real setups, a loss in mutual coherence with increasing interferometer delay T_{LDV} occurs.

The following model relates these crucial characteristics of heterodyning via offset-locked lasers. For simplicity, the deterministic phase variations φ_{vib} from the Doppler effect are omitted which superimpose on the stochastic phase fluctuations. Thus, the photocurrent signal from (1) at the photodetectors PD1 and PD2 is

$$i(t, T_{\text{LDV}}) = \hat{i} \cos [2\pi \nu_c (t + T_{\text{LDV}}) + \Delta\varphi_{\text{SM}}(t, T_{\text{LDV}})] \quad (6)$$

with the accumulated differential-phase fluctuation during the time interval $[t; t + T_{\text{LDV}}]$:

$$\Delta\varphi_{\text{SM}}(t, T_{\text{LDV}}) = \varphi_{\text{S}}(t + T_{\text{LDV}}) - \varphi_{\text{M}}(t) \quad (7)$$

due to the interferometer delay T_{LDV} . Assuming ergodic noise processes, the autocorrelation function $R_{i,\text{PN}}$ of the photocurrent signal $i(t, T_{\text{LDV}})$ in (6), solely from phase noise (PN), with lag τ is

$$R_{i,\text{PN}}(\tau, T_{\text{LDV}}) = \lim_{T \rightarrow \infty} \frac{1}{2T} \int_{-T}^T i(t + \tau, T_{\text{LDV}}) i^*(t, T_{\text{LDV}}) dt$$

$$\begin{aligned} &= \langle i(t + \tau, T_{\text{LDV}}) i^*(t, T_{\text{LDV}}) \rangle_t \\ &= \frac{\hat{i}^2}{2} \cos(2\pi \nu_c \tau) \langle \exp[j\Phi(t, T_{\text{LDV}}, \tau)] \rangle_t \end{aligned} \quad (8)$$

with the accumulated phase difference

$$\Phi(t, T_{\text{LDV}}, \tau) = \Delta\varphi_{\text{SM}}(t + \tau, T_{\text{LDV}}) - \Delta\varphi_{\text{SM}}(t, T_{\text{LDV}}). \quad (9)$$

The emissions of both lasers result from a large number of independent spontaneous-emission events within the time interval $[t; t + T_{\text{LDV}}]$ [17]. Due to the central limit theorem [31], the accumulated phase difference Φ is assumed to follow a Gaussian statistics [32] with zero mean and the variance σ_{Φ}^2 . From this, the last term in (8) can be expressed with some calculation effort [32] yielding

$$\langle \exp[j\Phi(t, T_{\text{LDV}}, \tau)] \rangle_t = \exp\left[-\frac{\sigma_{\Phi}^2(T_{\text{LDV}}, \tau)}{2}\right]. \quad (10)$$

Exploiting the Wiener–Khintchine theorem [32], the photocurrent-PSD can be calculated from the Fourier transform of the photocurrent-autocorrelation function (8) with (10)

$$\begin{aligned} S_{i,\text{PN}}(f, T_{\text{LDV}}) &= \int_{-\infty}^{\infty} R_{i,\text{PN}}(\tau, T_{\text{LDV}}) \exp(-j2\pi f\tau) d\tau \\ &= \frac{\hat{i}^2}{2} \int_{-\infty}^{\infty} \exp\left[-\frac{\sigma_{\Phi}^2(T_{\text{LDV}}, \tau)}{2}\right] \cos(2\pi \nu_c \tau) \exp[-j2\pi f\tau] d\tau \end{aligned} \quad (11)$$

which is symmetric around the heterodyne-carrier frequency ν_c . Note that due the laser Doppler effect, the frequency difference to the heterodyne carrier $|f - \nu_c|$ corresponds to the vibration frequency f_{vib} of a harmonic sample motion.

The conversion of differential-phase noise into photocurrent-PSD allows to spectrally compare phase-noise contribution in (5) against the other noise sources (e.g. shot noise, thermal noise, quantization noise) in a convenient way. Further, the photocurrent-PSD is directly accessible in experiment with a spectrum analyzer.

3.2. Modeling the variance of the differential-phase noise of two-laser interferometers

The variance σ_{Φ}^2 of the accumulated phase difference Φ can be expressed with the underlying phase-noise processes from the two lasers by using (9) and (7). These noise processes are also represented by their autocorrelation function and the cross-correlation function describing the interdependence generated by the OPLL. Thus, the variance, considering zero mean, is

$$\begin{aligned}
\sigma_{\Phi}^2(T_{LDV}, \tau) &= \langle \Phi^2(t, T_{LDV}, \tau) \rangle_t \\
&= 2 \left[\langle \varphi_M^2(t) \rangle_t - \langle \varphi_M(t+\tau)\varphi_M(t) \rangle_t \right] \\
&\quad + 2 \left[\langle \varphi_S^2(t) \rangle_t - \langle \varphi_S(t+\tau)\varphi_S(t) \rangle_t \right] \\
&\quad - 4 \langle \varphi_S(t+T_{LDV})\varphi_M(t) \rangle_t \\
&\quad + 2 \langle \varphi_M(t+\tau)\varphi_S(t+T_{LDV}) \rangle_t \\
&\quad + 2 \langle \varphi_S(t+\tau+T_{LDV})\varphi_M(t) \rangle_t \\
&= 2 [R_{\varphi,MM}(0) - R_{\varphi,MM}(\tau)] \\
&\quad + 2 [R_{\varphi,SS}(0) - R_{\varphi,SS}(\tau)] \\
&\quad - 2 [2R_{\varphi,SM}(T_{LDV}) - R_{\varphi,SM}(T_{LDV} - \tau) \\
&\quad - R_{\varphi,SM}(T_{LDV} + \tau)].
\end{aligned} \tag{12}$$

Here, $R_{\varphi,MM}$ is the phase-autocorrelation function of the master laser φ_M and correspondingly $R_{\varphi,SS}$ for the slave laser. Moreover, the variance σ_{Φ}^2 depends on the phase-cross-correlation function $R_{\varphi,SM}$ between master and slave laser.

According to Wiener-Khinchine theorem [32], the phase-autocorrelation function $R_{\varphi,SS}(\tau)$ and the phase-PSD $S_{\varphi,SS}(f)$ form a Fourier pair. The analogous applies for the master laser. The phase-cross-correlation function $R_{\varphi,SM}$ also forms a Fourier pair with the (complex) phase-cross-PSD $S_{\varphi,SM}$. Furthermore, it holds [32] that $S_{\varphi}(f) = f^{-2} S_{\nu}(f)$ since frequency fundamentally is the derivation of phase. With these Fourier pairs and the LDV setup depicted in figure 1(b) (free-running master laser and locked slave laser), the variance from (12) yields

$$\begin{aligned}
\sigma_{\Phi}^2(T_{LDV}, \tau) &= 2 \int_{-\infty}^{\infty} S_{\varphi,MM}^{\text{fr}}(f) [1 - \cos(2\pi f\tau)] df \\
&\quad + 2 \int_{-\infty}^{\infty} S_{\varphi,SS}^{\text{lock}}(f) [1 - \cos(2\pi f\tau)] df \\
&\quad - 4 \int_{-\infty}^{\infty} S_{\varphi,SM}^{\text{lock}}(f) \exp(j2\pi f T_{LDV}) \\
&\quad \times \left[1 - \frac{\exp(-j2\pi f\tau) + \exp(j2\pi f\tau)}{2} \right] df \\
&= 4 \int_{-\infty}^{\infty} S_{\nu,MM}^{\text{fr}}(f) \frac{\sin^2(\pi f\tau)}{f^2} df \\
&\quad + 4 \int_{-\infty}^{\infty} S_{\nu,SS}^{\text{lock}}(f) \frac{\sin^2(\pi f\tau)}{f^2} df \\
&\quad - 8 \int_{-\infty}^{\infty} S_{\nu,SM}^{\text{lock}}(f) \exp(j2\pi f T_{LDV}) \frac{\sin^2(\pi f\tau)}{f^2} df
\end{aligned} \tag{13}$$

with the frequency-PSD $S_{\nu,SS}^{\text{lock}}$ of the slave laser in lock and the frequency-cross-PSD $S_{\nu,SM}^{\text{lock}}$ between slave and master laser in lock. We further assume white frequency-PSD for both lasers ($2\pi S_{\nu,M}^{\text{fr}} = \Delta\nu_M$), which is generated by spontaneous emission with the laser linewidth $\Delta\nu_M$ [32]. This laser frequency noise is equivalent to a random-walk process for the laser phase.

4. Theoretical model validation and discussion

4.1. Validation for common interferometric configurations

Before expressing the cross correlation from the phase coupling in the OPLL, the model is validated for well-known special cases. For the special case of the independent laser sources (OPLL out-of-lock), the cross correlation vanishes and the photocurrent-PSD in (11) with (13) converges to a Lorentz function with the summed linewidth ($\Delta\nu_M + \Delta\nu_S$)

$$S_i^{\text{no lock}}(f) \approx \frac{i^2}{2} \frac{2\pi(\Delta\nu_M + \Delta\nu_S)}{[\pi(\Delta\nu_M + \Delta\nu_S)]^2 + 4\pi^2(f - \nu_c)^2} \tag{14}$$

which is consistent with the literature [32]. Due to the assumed (wide-sense) stationarity, the frequency difference ν_c in this special case remains stable despite no lock. However, in reality one has to deal with an unstable difference frequency or drift.

For the case of ideally offset-locked lasers (or a single laser source with ideal frequency shifting), relation (13) converges to the well-known experiment of delayed self-heterodyne mixing [17] (since $S_{\nu,SS}^{\text{lock}} \approx S_{\nu,MM}^{\text{fr}}$ and $S_{\nu,SM}^{\text{lock}} \approx S_{\nu,MM}^{\text{fr}}$). In this experiment, the photocurrent-PSD results in a distinct carrier at ν_c for zero delay T_{LDV} and a characteristic shape of the noise level dependent on the interferometer delay. For large interferometer delays, the photocurrent-PSD converges to the uncorrelated or unlocked special case expressed by (14).

4.2. Differential-phase variance for heterodyning via offset-locked lasers and discussion

The OPLL correlates the laser phases and, thus, the cross correlation of the laser phases is dependent on the OPLL transfer function $H(f)$ in steady state (see section 2.2). From control theory [33], it follows from (3) that the phase-cross-PSD $S_{\varphi,SM}^{\text{lock}}$ results from the multiplication of the OPLL transfer function and the (input) phase-PSD of the master laser $S_{\varphi,MM}^{\text{fr}}$.

Further, the (output) phase-PSD of the locked slave laser from the complete transfer function (see (3)) is

$$S_{\varphi,SS}^{\text{lock}}(f) \approx S_{\varphi,MM}^{\text{fr}}(f) |H(f)|^2 + S_{\varphi,SS}^{\text{fr}}(f) |1 - H(f)|^2. \tag{15}$$

Due to the linearized OPLL operation in (3), the filtered Gaussian phase-noise processes remain Gaussian [31]. With these relations, the variance of the phase difference of (13) becomes

$$\begin{aligned}
\sigma_{\Phi}^2(T_{LDV}, \tau) &\approx 2\pi \Delta\nu_M \tau^2 \int_{-\infty}^{\infty} \left[1 - 2H(f) \exp(j2\pi f T_{LDV}) \right. \\
&\quad \left. + |H(f)|^2 \right] \frac{\sin^2(\pi f\tau)}{\pi^2 f^2 \tau^2} df \\
&\quad + 2\pi \Delta\nu_S \tau^2 \int_{-\infty}^{\infty} |1 - H(f)|^2 \frac{\sin^2(\pi f\tau)}{\pi^2 f^2 \tau^2} df.
\end{aligned} \tag{16}$$

Relation (13) can be solved analytically for the special case of a 1st-order OPLL without intra-loop delay ($G_{OL}(s) = 2\pi f_L/s$) and zero interferometer delay, yielding

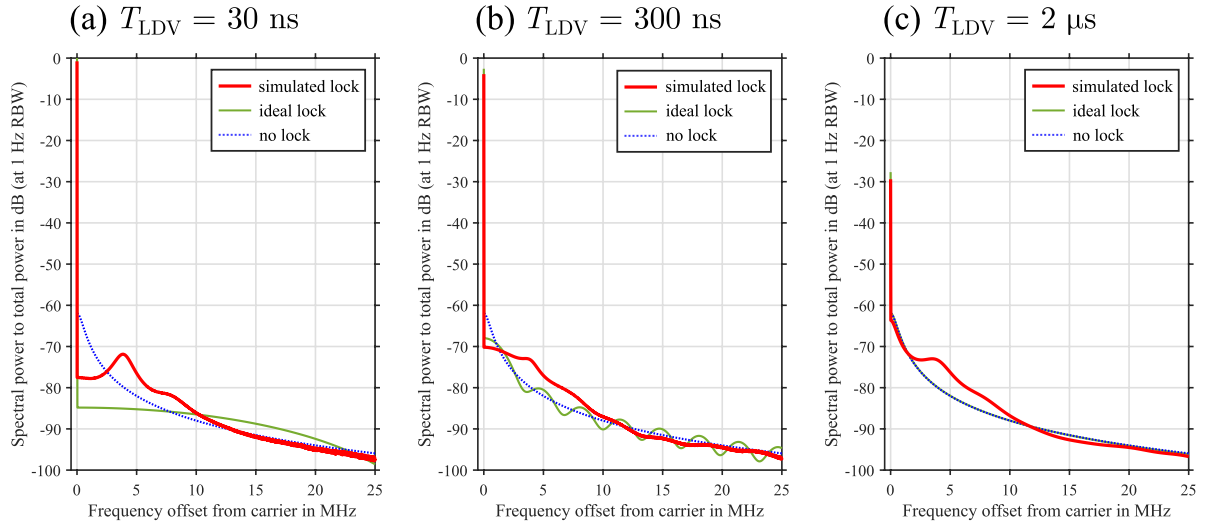


Figure 3. Simulated photocurrent-PSD $S_{i,PN}$ (red) of the interference of a phase-locked lasers with a linewidth of $\Delta\nu_M = \Delta\nu_S = 500$ kHz by a 1st-order OPLL with open-loop bandwidth $f_L = 3$ MHz (at 0 dB gain) and phase margin of 30 deg. The interference is shown for interferometer delays T_{LDV} of (a) 30 ns, (b) 300 ns, and (c) 2 μ s. The Lorentz function (dotted-blue) for the free-running case and the case of ideal coupling with unlimited bandwidth (green) are plotted as reference. The spectral power is normalized to the total interference-signal power.

$$\sigma_{\Phi}^2(T_{LDV} = 0, \tau = 0) = \pi(\Delta\nu_M + \Delta\nu_S)f_L^{-1}. \quad (17)$$

This is in accordance with the model predictions of other groups [17, 27]. However, our model is not limited to this simplification of the OPLL transfer function.

From relation (13), we state the following recommendations for the generation of a predominant heterodyne carrier for laser-Doppler vibrometry with a high suppression of the differential-phase noise:

- The loop bandwidth f_L must be larger than the summed laser linewidth ($\Delta\nu_M + \Delta\nu_S$) for proper suppression of the frequency or phase noise. Primarily, stability of the OPLL defines this relation and is in accordance to [17, 27].
- The interferometer delay T_{LDV} must be as low as possible. A predominant interference signal is achieved, if the delay $\exp(j2\pi f T_{LDV})$ remains small within the loop bandwidth f_L . We propose that $2\pi f_L T_{LDV} < 1$, which is equivalent to the coherence time of a single laser source. For a loop bandwidth of 3 MHz this requires an interferometer delay of $T_{LDV} < 53$ ns corresponding to an optical path difference of OPD < 16 m. This relation further shows that higher loop bandwidths require more effort in equalizing the beam paths of the interferometer setup.

5. Model validation with numerical simulation and experiment

5.1. Results from the numerical simulation

For the comparison to the real experiment, we conducted a numerical simulation of the resulting photocurrent-PSD in (11) with a differential-phase variance from (16) generated by a 1st-order-loop OPLL ($F(s) = \text{const.}$) with an open-loop

bandwidth (at 0 dB gain) of $f_L = 1$ MHz and a phase margin of 30 deg (due to intra-loop delays).

The simulation results in figure 3 show that, for minor delays, the differential-phase noise and, thus, the photocurrent-PSD is strongly damped by the OPLL within the loop bandwidth f_L around the carrier ν_c (red curve in figure 3(a)), in comparison to the out-of-lock case, which forms the Lorentz function (blue), see (14). Outside the loop bandwidth, the photocurrent-PSD approximately follows the Lorentz function of the out-of-lock case. The low phase margin generates noise peaking at the frequency distance $\nu_c \pm f_L$ and harmonics. With rising interferometer delay T_{LDV} , the photocurrent-PSD roughly follows the behavior of a delayed-self-heterodyne-mixing experiment (dotted-green), which results an increase of the noise level within the loop bandwidth with increasing interferometer delay. With a further increase of the interferometer delay (figure 3(c)), the heterodyne carrier collapses towards the out-of-lock case (blue).

The heterodyne-carrier strength is decisive for the phase modulation from the Doppler effect. Since the stated requirements in section 4.2 can usually be met for laboratory setups, the heterodyne-carrier collapse for the simulated case is less than 1 dB (figure 3(a)).

5.2. Experimental model validation

Our LDV with offset-locked visible semiconductor lasers is able to generate a heterodyne carrier up to frequencies ≤ 1.4 GHz and measure vibration frequencies < 700 MHz [26, 34]. Both is mainly limited by the bandwidth of commercial photodetectors with a single photosensitive element. Commercial balanced photodetectors with two photosensitive elements are restricted to even smaller bandwidths.

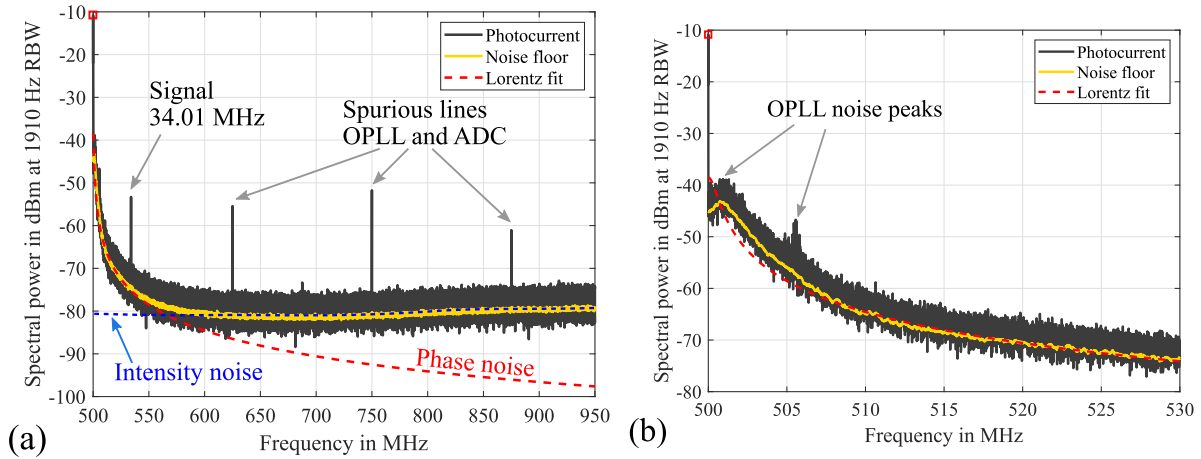


Figure 4. (a) Experimental power spectrum (upper sideband) of the photocurrent with our LDV setup with two offset-locked semiconductor lasers. The vibration measurement was conducted on an SAW excited at 34.01 MHz with a heterodyne carrier at 500 MHz (red square). The noise floor (yellow) was estimated by a moving median, for which a Lorentz function with 1 MHz width was fitted. (b) Zoom to the power spectrum near the heterodyne carrier showing noise peaking.

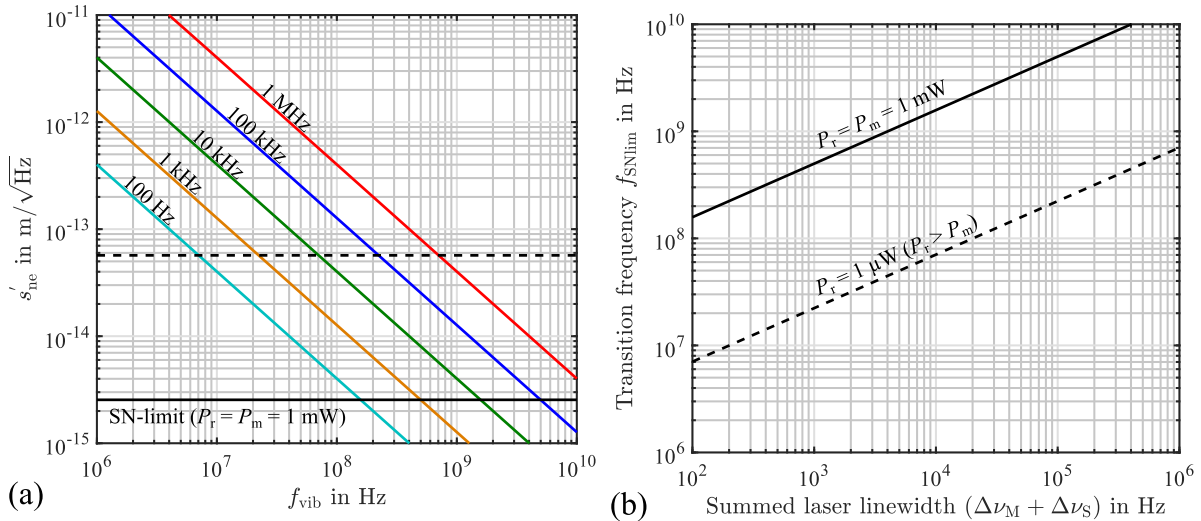


Figure 5. (a) Noise-equivalent vibration amplitude $\hat{s}'_{ne}(f_{\text{vib}})$ limited by phase noise at several (summed) laser linewidths. Shot-noise limit are given for $P_r = P_m = 1 \text{ mW}$ (black-line) and $P_m = 1 \mu\text{W}$ ($P_r > P_m$) (black-dashed). (b) Transition frequency to shot-noise-limited detection f_{SNlim} in dependence on the summed linewidth $(\Delta\nu_M + \Delta\nu_S)$ of the offset-locked lasers for powers of the interfering beam (for $\chi = 1$ and $S = 0.5 \text{ A/W}$, and $\lambda = 632 \text{ nm}$).

In previous experiments, we showed the capability of unambiguous vibration reconstruction in amplitude and phase exemplary with vibration measurements on a SAW filter excited at 34.01 MHz [34]. Intensity and phase noise of the semiconductor lasers limit the vibration amplitude resolution (figure 4(a)). However, the achieved signal-to-noise ratio of more than 100 dB at 1 Hz RBW for vibration frequencies higher than 50 MHz already provides noise-equivalent vibration amplitudes less than $1 \text{ pm}/\sqrt{\text{Hz}}$ (see (4)), which is suitable for RF-MEMS testing.

The measured photocurrent-PSD from our experiment (figure 4(b)) validates the predicted decay with the Lorentz function of the summed laser linewidths $< 1 \text{ MHz}$ from the numerical simulations. Furthermore, the experiments show the spectral noise peaking at the loop bandwidth and harmonics due to low phase margin of the OPLL.

The path difference in the experiment is $\sim 1.5 \text{ m}$, which results in an interferometer delay of $\sim 5 \text{ ns}$. Regarding the loop bandwidth of $\sim 3 \text{ MHz}$, the stated requirements for a predominant carrier are met (see section 4.2). The differential-phase noise within the loop bandwidth is damped to $\sim 69 \text{ dBc}$ (at 1 Hz RBW), which is less than in the numerical simulation (76 dBc). This might arise from neglected noise processes in our model.

5.3. Transition to shot-noise-limited LDV measurement

In interferometry, typically shot-noise-limited measurement is aspired to achieve highest vibration-amplitude resolution. However, for heterodyning with offset-locked lasers, the photocurrent-PSD is dominated by the differential-phase noise at vibration frequencies up to the range of the loop bandwidth.

Outside the loop bandwidth, the photocurrent-PSD follows the decay of the Lorentz function. Thus, the noise-equivalent vibration amplitude from (4) also decreases with higher vibration frequencies shown in figure 5(a). Therefore, a transition frequency f_{SNlim} might exist within the electronic bandwidth where shot noise dominates the signal-to-noise ratio in (5) over the phase-noise contribution (estimated with (14)):

$$S_{i,\text{SN}} > S_{i,\text{PN}}(\nu_c \pm f_{\text{vib}}) \approx S_i^{\text{no lock}}(f_{\text{vib}}) \\ 2q_e \mathcal{S}(P_m + P_r) > 2\chi^2 \mathcal{S}^2 P_m P_r \frac{2\pi(\Delta\nu_M + \Delta\nu_S)}{[\pi(\Delta\nu_M + \Delta\nu_S)]^2 + 4\pi^2 f_{\text{vib}}^2} \quad (18)$$

with the elementary charge q_e and photocurrent amplitude \hat{i} from (1). From this inequation, the shot-noise-limited detection can theoretically be performed for vibration frequencies:

$$f_{\text{vib}} > f_{\text{SNlim}} \approx \left[\frac{\chi^2 \mathcal{S}}{2\pi q_e} \frac{P_m P_r}{P_m + P_r} (\Delta\nu_M + \Delta\nu_S) \right]^{1/2}. \quad (19)$$

Figures 5(a) and (b) show that with narrow laser linewidths the transition frequency f_{SNlim} to shot-noise-limited detection decreases. Furthermore, the Lorentz function from phase noise is dependent on the interference signal, whereas the shot noise scales with the detected laser power. With increasing power of the interfering beams, the signal and phase noise experience a higher (coherent) gain than the shot noise, requiring even narrower laser linewidths for shot-noise-limited detection. For a shot-noise-limited detection at vibration frequencies above 1 GHz and 1 mW power each (on the detectors), the summed linewidth of the offset-locked lasers must be less than 4 kHz. Thus, the broad laser linewidths of semiconductor lasers inhibit shot-noise-limited detection at several gigahertz.

For surfaces with low reflectivity ($P_m \ll P_r$), the transition frequency f_{SNlim} approximately becomes independent from the power of the reference beam P_r (the same holds for s'_{ne} [3]). Thus, the transition frequency is decreased for lower measurement power P_m , which goes along with a worsened vibration-amplitude resolution.

6. Conclusion and outlook

We presented a comprehensive model for estimating the noise-equivalent vibration-amplitude resolution of a laser-Doppler vibrometer employing heterodyning with two offset-locked lasers. Therefore, the model of the differential-phase noise includes the laser linewidths, the OPLL transfer function, and the interferometer delays.

The model predicts a worse vibration-amplitude resolution for frequencies up to the OPLL bandwidth compared to conventional, shot-noise-limited vibrometers. However, outside the loop bandwidth, the noise-equivalent vibration amplitude decreases and can achieve shot-noise-limited resolution. From our model, we derive the transition frequency of the phase-noise-limited to shot-noise-limited detection. Moreover, the

model helps to compare the contribution of all usual noise sources of LDVs with the differential-phase noise of the proposed heterodyning technique. Experimental data from our realized LDV setup with offset-locked semiconductor lasers validated the model predictions including the spectral noise peaking.

Furthermore, the model allows to estimate the collapse of the heterodyne-carrier when the mutual coherence vanishes due to optical path differences within the interferometer setup. We give design rules for the maximum path difference for a neglectable carrier collapse. Thus, our model helps to derive general specifications for the lasers, the OPLL, and the interferometer setup with the proposed heterodyning technique for laser-Doppler-vibrometry

The future goal is to extend the measurement bandwidth of our LDV setup with offset-locked semiconductor lasers into the gigahertz regime using high-frequency single photodetectors. In addition, the experimental validation of the coherence collapse in the experiment is the subject of further investigations.

ORCID iD

Robert Kowarsch  <https://orcid.org/0000-0003-2000-7990>

References

- [1] Chambon H, Nicolay P, Moldaschl T, Zauner M, Humbert C, AminAwan A, Schiek M, Metzger T and Benjeddou A 2018 High frequency optical probe for BAW/SAW devices 2018 *IEEE Int. Ultrasonics Symp.* (Piscataway, NJ: IEEE) pp 1–4
- [2] Drain L E 1980 *The Laser Doppler Technique* (Chichester: Wiley)
- [3] Rembe C, Siegmund G, Steger H and Wörtge M 2007 Measuring MEMS in motion by laser doppler vibrometry *Optical Inspection of Microsystems* (Boca Raton, FL: CRC/Taylor & Francis) pp 245–92
- [4] Graebner J E 2000 Optical scanning interferometer for dynamic imaging of high-frequency surface motion 2000 *IEEE Int. Ultrasonics Symp. Proc.* pp 733–6 IEEE
- [5] Knuutila J V, Tikka P T and Salomaa M M 2000 Scanning Michelson interferometer for imaging surface acoustic wave fields *Opt. Lett.* **25** 613–15
- [6] Wagner J W 1990 Optical detection of ultrasound *Ultrasonic Measurement Methods (Physical Acoustics vol 19)* (Boston and London: Academic) ch 5, pp 201–66
- [7] Winter M, Fuser H, Bieler M, Siegmund G and Rembe C 2012 The problem of calibrating Laser-Doppler vibrometers at high frequencies *AIP Conf. Proc.* **1457** 165–75
- [8] Kowarsch R and Rembe C 2016 Modellierung der Auflösungssteigerung mittels photochromer Schichten für die nanoskopische Laser-Doppler-Vibrometrie XXX. *Messtechnisches Symp* (in German) pp 85–95
- [9] Kowarsch R, Geisler C, Egner A and Rembe C 2018 *Opt. Express* **26** 5327–41
- [10] Xu J and Stroud R 1992 *Acousto-optic Devices Principles Design and Applications* (New York: Wiley)
- [11] Martinussen H, Aksnes A and Engan H E 2007 Wide frequency range measurements of absolute phase and amplitude of vibrations in micro- and nanostructures by optical interferometry *Opt. Express* **15** 11370–84

- [12] Rembe C 2010 Employing applied mathematics to expand the bandwidth of heterodyne carrier signals with a small phase modulation index *Appl. Math. Comput.* **217** 1202–12
- [13] Goodwin F 1967 8.4 - A 3.39-micron infrared optical heterodyne communication system *IEEE J. Quantum Electron.* **3** 524–31
- [14] Gliese U, Nielsen T N, Bruun M, Lintz Christensen E, Stubkjaer K E, Lindgren S and Broberg B 1992 *IEEE Photonics Technol. Lett.* **4** 936–8
- [15] Kikuchi K 2016 Fundamentals of coherent optical fiber communications *J. Lightwave Technol.* **34** 157–79
- [16] Satyan N, Vasilyev A, Rakuljic G, Leyva V and Yariv A 2009 Precise control of broadband frequency chirps using optoelectronic feedback *Opt. Express* **17** 15991–9
- [17] Satyan N, Liang W and Yariv A 2009 Coherence cloning using semiconductor laser optical phase-lock loops *IEEE J. Quantum Electron.* **45** 755–61
- [18] Deninger A J, Göbel T, Schönherr D, Kinder T, Roggenbuck A, Köberle M, Lison F, Müller-Wirts T and Meissner P 2008 Precisely tunable continuous-wave terahertz source with interferometric frequency control *Rev. Sci. Instrum.* **79** 044702
- [19] Thorpe J I, Maghami P and Livas J 2011 Time domain simulations of arm locking in LISA *Phys. Rev. D* **83** 122002
- [20] Kwee P *et al* 2012 Stabilized high-power laser system for the gravitational wave detector advanced LIGO *Opt. Express* **20** 10617–34
- [21] Santarelli G, Clairon A, Lea S N and Tino G M 1994 Heterodyne optical phase-locking of extended-cavity semiconductor lasers at 9 GHz *Opt. Commun.* **104** 339–44
- [22] Wynands R, Coste O, Rembe C and Meschede D 1995 How accurate is optical second-harmonic generation? *Opt. Lett.* **20** 1095
- [23] Holzwarth R, Udem T, Hänsch T W, Knight J C, Wadsworth W J and Russell P S 2000 Optical frequency synthesizer for precision spectroscopy *Phys. Rev. Lett.* **85** 2264–7
- [24] Sternkopf C, Diethold C, Gerhardt U, Wurmus J and Manske E 2012 Heterodyne interferometer laser source with a pair of two phase locked loop coupled He–Ne lasers by 632.8 nm *Meas. Sci. Technol.* **23** 074006
- [25] Kowarsch R, Te R and Rembe C 2018 Laser-Doppler vibrometry with variable GHz heterodyne carrier via frequency-offset lock *J. Phys.: Conf. Ser.* **1149** 012016
- [26] Kowarsch R and Rembe C 2018 Laser-Doppler vibrometry with variable GHz heterodyne carrier via frequency-offset lock *Proc. SPIE* **107490** 107490A
- [27] Liang J, Zhang R and Sun N 2019 Affection of optical phase-locked loop on the coherence properties improving of laser *Opt. Laser Technol.* **109** 94–8
- [28] Wolf E 2007 Introduction to the theory of coherence and polarization of light (Cambridge: Cambridge University Press)
- [29] Paul H 1986 Interference between independent photons *Rev. Mod. Phys.* **58** 209–31
- [30] Gardner F M 2005 *Phaselock Techniques* 3rd ed (Hoboken, NJ: Wiley-Interscience)
- [31] Goodman J W 2000 *Statistical Optics Wiley Classics Library* (New York and Chichester: J. Wiley)
- [32] Riehle F 2004 *Frequency standards: Basics and Applications* (Weinheim: Wiley-VCH)
- [33] Unbehauen H 1988 *Regelungstechnik III: Identifikation, Adaption, Optimierung* 3rd ed (Braunschweig/Wiesbaden: Vieweg)
- [34] Kowarsch R and Rembe C 2019 Heterodyne laser-Doppler vibrometer with frequency-offset-locked diode lasers for vibration analysis of SAW filters *Tech. Mess. - ATM* **86** 27–31